BIOCYBERNETICS AND BIOMEDICAL ENGINEERING 42 (2022) 695–706

Available at www.sciencedirect.com

ScienceDirect

journal homepage: www.elsevier.com/locate/bbe

Original Research Article

Dual-channel asymmetric convolutional neural network for an efficient retinal blood vessel segmentation in eye fundus images

Yanan Xu, Yingle Fan *

Laboratory of Pattern Recognition and Image Processing, Hangzhou Dianzi University, Hangzhou, China

ARTICLE INFO

Article history:
Received 30 October 2021
Received in revised form
8 May 2022
Accepted 9 May 2022
Available online 24 May 2022

Keywords:
Retinal blood vessel segmentation
2D Gabor filter
Convolutional neural network
Dilated convolution
Feature fusion

ABSTRACT

The morphological properties of retinal vessels are closely related to the diagnosis of ophthalmic diseases. However, many problems in retinal images, such as complicated directions of vessels and difficult recognition of capillaries, bring challenges to the accurate segmentation of retinal blood vessels. Thus, we propose a new retinal blood vessel segmentation method based on a dual-channel asymmetric convolutional neural network (CNN). First, we construct the thick and thin vessel extraction module based on the morphological differences in retinal vessels. A two-dimensional (2D) Gabor filter is used to perceive the scale characteristics of blood vessels after selecting the direction of blood vessels; thereby, adaptively extracting the thick vessel features characterizing the overall characteristics and the thin vessel features preserving the capillaries from fundus images. Then, considering that the single-channel network is unsuitable for the unified characterization of thick and thin vessels, we develop a dual-channel asymmetric CNN based on the U-Net model. The MainSegment-Net uses the step-by-step connection mode to achieve rapid positioning and segmentation of thick vessels; the FineSegment-Net combines dilated convolution and the skip connection to achieve the fine extraction of thin vessels. Finally, the output of the dual-channel asymmetric CNN is fused and coded to combine the segmentation results of thick and thin vessels. The performance of our method is evaluated and tested by DRIVE and CHASE_DB1. The results show that the accuracy (Acc), sensitivity (SE), and specificity (SP) of our method on the DRIVE database are 0.9630, 0.8745, and 0.9823, respectively. The evaluation indexes Acc, SE, and SP of the CHASE_DB1 database are 0.9694, 0.8916, and 0.9794, respectively. Additionally, our method combines the biological vision mechanism with deep learning to achieve rapid and automatic segmentation of retinal vessels, providing a new idea for diagnosing and analyzing subsequent medical images.

* Corresponding author at: Laboratory of Pattern Recognition and Image Processing, Hangzhou Dianzi University, Hangzhou 310018, China.
E-mail address: fan@hdu.edu.cn (Y. Fan).
https://doi.org/10.1016/j.bbe.2022.05.003

1. Introduction

Ophthalmic diseases such as diabetic retinopathy (DR), glaucoma, and age-related macular degeneration can easily change the width, bifurcation, and tortuosity of retinal blood vessels, which can lead to insufficient blood supply in patients' eyes for a long time and even blindness [1]. In recent years, computer diagnostic systems [2] have been widely used to automatically segment and analyze retinal vascular structures, which effectively assists physicians to screen and monitor the corresponding ophthalmic diseases. However, since the acquired retinal images can be affected by blood vessel thickness, low contrast, and pathological noise, it is not easy to distinguish the interference between capillaries and complex backgrounds during the segmentation process, causing the complexity and low precision of blood vessel segmentation. Additionally, the performance of existing segmentation methods is poor, especially for capillary segmentation. The main reasons are summarized as follows:

1. Over-simplified approaches. Retinal blood vessels are characterized by intricate directions and highly imbalanced pixel ratios. However, existing methods [3,4] weaken the orientation selection and multi-scale perception of retinal vessels. In particular, there are significant morphological differences between thick and thin vessels, and the same mode should not be used for their representation.
2. Lack of targeted network design. To simplify the network structure and enhance the detection performance, existing methods [5,6] increase the depth of the single-channel network to identify the thick and thin vessel features. However, a large number of convolution and pooling operations will reduce the detection speed and make detailed information lost and difficult to recover in the sampling operation.
3. Lack of relevance between convolutional levels. Existing methods [7,8] use only the channel number combination to achieve feature fusion in the training process. Although thick vessels can be identified, the characteristics of thin vessels are inevitably ignored.

Therefore, this study focuses on how to accurately and efficiently segment thick and thin vessels in retinal images. Inspired by the multi-channel parallel processing mechanism of visual information, we propose a retinal vessel segmentation method based on a dual-channel asymmetric convolutional neural network (CNN), which is based on the preprocessing of orientation and scale features of retinal images. An asymmetrical CNN, MainSegment-Net and FineSegment-Net, are constructed in the proposed method according to the characteristics of thick and thin vessels. The segmentation results of the two channels are fused to achieve complementarity of detailed information. The main contributions of this study are as follows:

1. The thick and thin vessel extraction module was constructed. After the vessel direction selection, a 2D Gabor filter was used to obtain multi-scale vascular feature maps. Additionally, the vessel feature maps were extracted adaptively according to the characteristics of thick and thin vessels to enhance the direction selection and multi-scale perception of retinal vessel images.
2. An asymmetric CNN model was constructed. MainSegment-Net introduced a step-by-step connection mode for sampling operations to simplify the convolutional layer to achieve rapid positioning and segmentation of thick vessels. FineSegment-Net combined dilated convolution and the skip connection model to effectively compensate for thin vessels, that are not easily restored by upsampling during the downsampling process.
3. A dual-channel information fusion method was proposed. FineSegment-Net was used to supplement the information of thin vessels ignored in the segmentation process of MainSegment-Net to improve the efficiency and accuracy of the retinal blood vessel segmentation.

2. Review of related studies

In view of the challenges in the segmentation technology of the retinal vessel, existing methods for segmenting retinal vessels are divided into two categories: supervised and unsupervised [9]. Unsupervised methods do not rely on any labeled training samples. They mainly use matched filters (MFs), blood vessel tracking, and morphological processing for segmentation. Chaudhuri et al. [10] took the lead in designing the gray distribution characteristics of the cross-section of the blood vessel based on the Gaussian MF, and constructed multi-directional templates to identify the piecewise linear segments of retinal blood vessels. Hugo et al. [11] combined 2D Gabor filter and halfwave rectification for extracting retinal vessels to improve segmentation efficiency for low-contrast and narrow blood vessels. However, such a method is more sensitive to nonvascular areas and has poor segmentation accuracy for pixel points with low contrast. In the tracking methods [12], Delibasis et al. [13] used an automatic vessel tracing algorithm recursively to segment the whole vessel tree and calculate vessel diameter and orientation. Zhao et al. [14] further proposed a superpixel-based chain tracking method to segment retinal vessels, treating vessel regions with good and poor imaging quality differently. However, such a method is highly dependent on manually selected starting and ending points and cannot effectively segment the branch and intersection points of retinal vessels. Morphological methods [15] use morphological properties, such as curvature, connectivity, and width, to perform operations on retinal images, such as expansion and corrosion. However, these morphological structures are easily interfered by fundus lesions. Compared with unsupervised methods, supervised methods use the known training samples to construct the classifier and perform the pixel-level classification after extracting retinal vessel features using the k-nearest neighbor method [16], support vector machine (SVM), or deep neural network as classifiers [17]. Orlando et al. [18] introduced SVM based on the Fully Connected Conditional Random Field (FC-CRF) model to learn the method's parameters

and effectively segmented the slender structure of the fundus blood vessels. Fu et al. [19] combined the deep learning network with FC-CRF to improve the robustness of pathological region segmentation in fundus images. Although the above-supervised methods have good segmentation effect, they need manual pre-segmented fundus images as a reference and lacks clinical application adaptability.

Based on the significant effects of deep learning in visual recognition tasks, it provides a new idea for improving the accuracy of image segmentation. Since 2015, Fully Convolutional Neural Network (FCN) [20] has been widely used in the retinal vascular segmentation task, which achieves an end-to-end output and greatly reduces training times. The relatively rough design of FCN also accelerates the successive proposals of new network models, such as U-Net [21], CE-Net [22], and VSSC-Net [6]. Ronneberger et al. [21] proposed a symmetrical structure of the encoder–decoder model—U-Net, which used a contraction path that captures context information and a symmetrical expansion path that was accurately positioned to classify fundus blood vessel pixels accurately. Pan et al. [23] further proposed an ResUnet model that combined U-Net with residual learning strategies. The introduction of residual elements deepened the network depth and improved network performance. However, such a method is insufficient for pathological information or capillary segmentation. Some researchers [7,8] combined preprocessing and data expansion methods with deep learning models into hybrid methods. They used histogram equalization to enhance the contrast relationship between background and fundus blood vessels and designed CNN training to obtain blood vessels. However, these methods do not fully consider the correlation between network levels in the segmentation process, and the blood vessels are easily lost and cannot be compensated.

In summary, we propose an asymmetric CNN model for segmenting thick and thin vessels in digital fundus camera images. According to the characteristics of blood vessels, any channel is constructed and selected adaptively, which can effectively improve the network segmentation accuracy. The blood vessel information in dual-channel is also integrated to take advantages of their respective advantages and improve the performance and accuracy of blood vessel segmentation.

3. Principle of the algorithm

When the human brain perceives and processes visual information, it is not limited to a certain visual pathway but differentiates visual information and transmits it to a specific visual pathway for targeted processing and analysis [24]. Similarly, blood vessels with different widths in retinal images have different requirements for segmentation accuracy. For example, fine-grained features of thin vessels may not be easy to recover due to the loss of subsampling operation.

Therefore, we use a 2D Gabor filter to preprocess retinal vessels in multiple scales and directions to adaptively extract the thick vessel feature map characterizing the overall characteristics and the thin vessel feature map preserving capillaries, respectively used as the input of the dual-channel asymmetric CNN. Then, MainSegment-Net and FineSegment-Net corresponding to different characteristics are constructed. MainSegment-Net is based on convolution and pooling operations and adopts a step-by-step connection mode to reduce the information loss of thick vessels by simplifying the complementarity between convolution levels. However, FineSegment-Net has more information flow paths. The low-level feature maps after downsampling are subjected to parallel dilated convolution with different expansion rates and combined with the corresponding high-level feature maps after upsampling step-by-step segment blood vessels accurately. Finally, the information fusion is performed on the dual-channel network with asymmetric structure. In particular, the neglected details in MainSegment-Net are complemented by the capillary segmentation map to realize the information and advantage complementarities between dual-channel. The principle of the method proposed in this paper is shown in Fig. 1.

3.1. *Thick / thin vessel extraction module*

3.1.1. *Image preprocessing*

Considering that the grayscale difference between blood vessels and background in retinal image is relatively low, and the expansion operation of the region of interest can easily cause the loss of vascular information around the optic disk, we adopt the contrast-limited adaptive histogram equalization (CLAHE) algorithm [15] to enhance the contrast of the green channel in the retinal image. The vascular enhancement results are used as the input of the thick and thin vessel extraction module.

Fig. 2 shows the preprocessing process of retinal vessels. As shown in this figure, Fig. 2(a) represents the original image of the retina; Fig. 2(b) represents the green channel with the highest definition; Fig. 2(c) represents blood vessels after the expansion operation; Fig. 2 (d) represents the map of vascular enhancement after CLAHE treatment.

3.1.2. *Feature extraction*

Biological vision research has shown that a 2D Gabor filter can effectively describe the response of mammalian simple visual cortex cells, and it is usually used to perceive the image direction and scale information [25]. When capturing blood vessel features with arbitrary directions and different widths, the direction selectivity and perceived scale difference of a 2D Gabor filter help realize the difference extraction of retinal blood vessel pixels. Therefore, we use a 2D Gabor function with equal angular intervals to extract the blood vessel features, as shown in Eq. (1) [4].

$$\begin{cases} R_{\theta,\sigma,\varphi}(x,y) = \exp\left(-\frac{\tilde{x}^2+\gamma^2\tilde{y}^2}{2\sigma^2}\right)\cos\left(2\pi\frac{\tilde{x}}{\lambda}+\varphi\right) \\ r_{\theta_i,\sigma,\varphi}(x,y) = R_{\theta_i,\sigma,\varphi}(x,y) * f(x,y), i = 1,2,\cdots,12 \end{cases} \quad (1)$$

where $*$ represents the convolution operation; $f(x,y)$ represents the vascular enhancement image with size $H \times W$; $\theta_i \in [0,180°)$ represents different selected direction angles with an interval of 15°;γ,φ,σ, and $1/\lambda$ represent the ellipticity, phase angle, scale, and spatial modulation frequency of a 2D Gabor filter, respectively. The 2D Gabor odd–even symmetrical filter

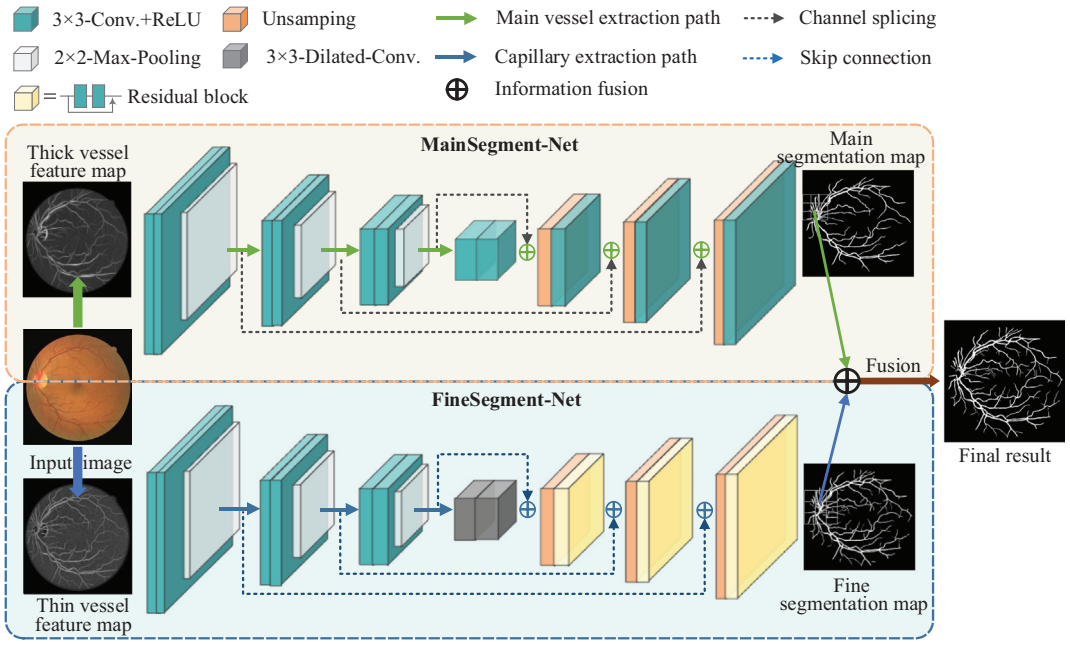

Fig. 1 – Principle of fundus image blood vessel segmentation method based on dual-channel asymmetric convolutional neural network.

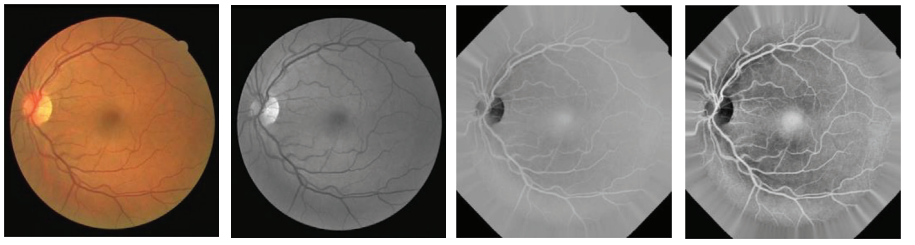

(a) Original image (b) Green channel (c) Vascular expansion (d) Vascular enhancement

Fig. 2 – Schematic diagram of image preprocessing.

with phase angle difference can simulate the multi-directional response of blood vessels, as shown in Eq. (2).

$$G_{\theta_i,\sigma}(x,y)=\sqrt{r_{\theta_i,\sigma,0}(x,y)^2+r_{\theta_i,\sigma,\ -\ 90^\circ}(x,y)^2} \tag{2}$$

Since the width and contrast characteristics of retinal blood vessels are not balanced, we consider the multi-scale azimuth characteristics of blood vessels according to Eq. (2). Blood vessel scales are divided with an interval of 0.5 within the scale range, and the maximum value of multi-directional response is extracted at each scale, as shown in Eq. (3).

$$\hat{G}_{\theta_i,\sigma_j}(x,y)=\max\left\{G_{\theta_i,\sigma_j}(x,y)|i=1,2,\cdots,12;j=1,2,\cdots,6\right\} \tag{3}$$

According to image entropy, the thick and thin vessel features are extracted separately in$\hat{G}_{\theta_i,\sigma_j}(x,y)$. Here, the response corresponding to the maximum entropy value is selected as the thin vessel feature map. The thick blood vessel branches show a divergent distribution from coarse to fine; the remaining scale information is fused to obtain the thick vessel feature map, as shown in Eqs. (4) and (5).

$$ENT_j=-\sum_{x=1}^{H}\sum_{y=1}^{W}\hat{G}_{\theta_i,\sigma_j}(x,y)\log\hat{G}_{\theta_i,\sigma_j}(x,y) \tag{4}$$

$$\begin{cases}\tilde{G}_{thin}(x,y)=\widehat{G}_{\theta_i,\sigma_{j_{max}}}(x,y)\\ \tilde{G}_{thick}(x,y)=\sum\limits_{\substack{j=1\\ j\neq j_{max}}}^{6}\left(|\widehat{G}_{\theta_i,\sigma_j}(x,y)|\right)\end{cases} \tag{5}$$

where ENT_j represents the 2D entropy function of the image. The response scale corresponding to its maximum value is$\sigma_{j_{max}}$; $\tilde{G}_{thin}(x,y)$ and $\tilde{G}_{thick}(x,y)$ represent the thin vessel feature map and thick vessel feature map, respectively.

3.2. *Main vessel segmentation network*

The receptive cell field in the V1 region of the visual system has a sparse response characteristic. When the visual information flow is transmitted from low to high level, the characteristic can reduce the redundancy of visual information and extract the essential features to highlight the overall characteristics of image objects [26]. Similarly, the neural network can simulate the hierarchical structure of the visual system

and realize the sparse coding of retinal images by utilizing the high efficiency of the convolution and sampling operations in the computation. Therefore, we construct MainSegment-Net based on the thick vessel feature map $\tilde{G}_{thick}(x,y)$ to quickly locate and segment thick vessels.

MainSegment-Net consists of an encoder and a decoder, and the main structure is shown in Fig. 3. The convolutional layers of MainSegment-Net are simplified to improve the perceived speed of the thick vessel features since thick vessels in $\tilde{G}_{thick}(x,y)$ have different widths but clear veins. Additionally, based on the correlation between convolutional layers, a step-by-step connection mode is introduced to reduce the loss of vascular features caused by pooling operation with information complementation between convolutional blocks. The encoder designed by MainSegment-Net consists of three modules. Each module consists of two layers of 3×3 convolutional blocks with a step length of 1 and a layer of 2×2 with a maximum pooling step of 2. The decoder corresponding to the downsampling operation consists of three modules. Each module consists of two layers of 3×3 convolution blocks with a step size of 1 and an upsampling. The number of convolution kernels in each module layer is the same, which are 64, 128, 256, 256, 128, and 64 in turn. After processing $\tilde{G}_{thick}(x,y)$ with MainSegment-Net, the main segmentation map $F_{main}(x,y)$ is obtained.

3.3. *Fine vessel segmentation network*

Visual perception is an essential attributes for the visual system to capture the target. It can guide the fixation point to the image target according to context information and rely on the expansion of the visual receptive field to capture a more detailed information [27]. Similarly, residual blocks are used in the neural network to replace part of the convolution blocks to improve the utilization efficiency of thin vessel features. Additionally, dilated convolution is introduced to expand the receptive field and strengthen the correlation between information elements. Therefore, we construct FineSegment-Net based on the thin vessel feature map $\tilde{G}_{thin}(x,y)$ to achieve fine segmentation of thin vessels while ensuring low loss of blood vessel information.

FineSegment-Net consists of an encoder and a decoder. However, due to the slender shape of thin vessels and its width of only a few pixels, its morphological attributes cannot be segmented by the simplified MainSegment-Net. Thus, FineSegment-Net is asymmetric with MainSegment-Net in structure. We add a skip connection module between the encoder and decoder since thin vessels in $\tilde{G}_{thin}(x,y)$ are not easy to segment and are easy to lose. We use three parallel dilated convolutions to make the cross-stage connection of the corresponding encoder and decoder. The purpose is to ensure that each layer's vascular feature map is obtained by splicing the feature channels of the next layer and the corresponding downsampling operation in the upsampling process. Simultaneously, to expand the range of feature extraction, the expansion rate d of the network is increased based on the convolution kernel. The expanded convolution kernel's size and the dilated convolution output are shown in Eq. (6).

$$\begin{cases} n_i = k + (k-1) \times (d_i - 1), i = 1,2,3 \\ z_i = \left[\frac{g+2p-n_i}{s}\right] + 1 \end{cases} \tag{6}$$

where k represents the size of the convolution kernel; d_i represents different expansion rates, which are 1, 2, and 4. The corresponding dilated convolution kernel is n_i; g represents the input of dilated convolution, p represents the number of pixels filled in the convolution process, and s represents the moving step. After three parallel dilated convolution processing, the output z_i of the parallel dilated convolution completes feature fusion through feature splicing (Fig. 4). The splicing result is output by the encoder after being processed by the skip connection module.

Fig. 5 shows the main structure of FineSegment-Net. The encoder designed in FineSegment-Net consists of four modules. The first three modules consist of two layers of 3×3 convolution blocks with a step size of 1, a skip connection module, and a layer of 2×2 maximum pooling with a step size of 2. The fourth module consists of two layers of 3×3 dilated convolution blocks with a step size of 1. The decoder consists of three modules. Each module consists of an upsampling and a residual block; the residual block contains two two-layer 3×3 convolution blocks with a step size of 1. The number of convolution cores at each module layer is

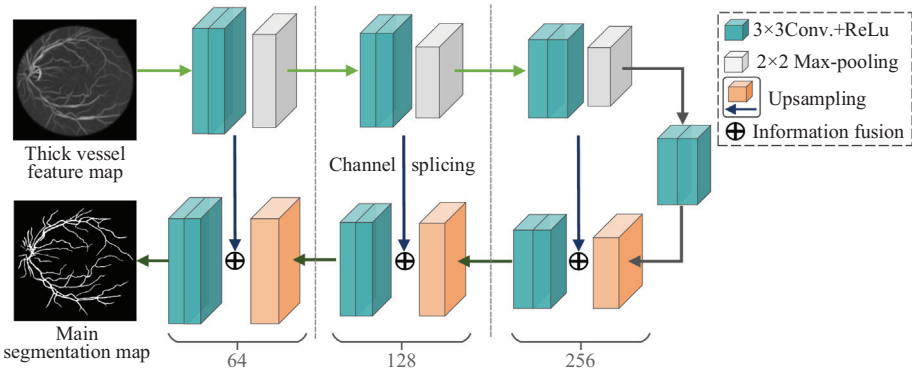

Fig. 3 – Structure diagram of MainSegment-Net.

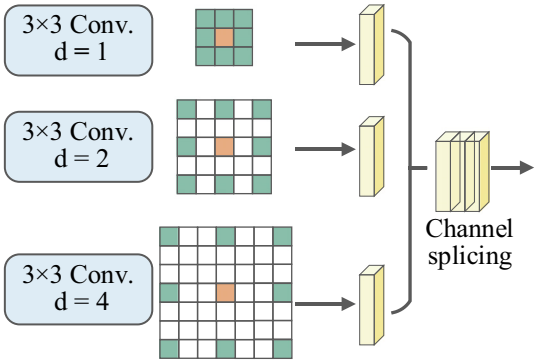

Fig. 4 – Schematic diagram of the skip connection module.

the same, which are 64, 128, 256, 512, 256, 128, and 64 in turn. To compensate for the details that cannot be restored in the decoding process, the feature information obtained from the thin vessel feature map $\tilde{G}_{thin}(x,y)$ through the encoder is gradually integrated into the corresponding decoder to obtain a more detailed segmentation effect and the fine segmentation map $F_{fine}(x,y)$.

3.4. *Dual-channel fusion coding*

Considering the multi-channel parallel processing mechanism of information on the visual path, the $\tilde{G}_{thick}(x,y)$ and $\tilde{G}_{thin}(x,y)$ processed by 2D Gabor filter are input into MainSegment-Net and FineSegment-Net, respectively, to obtain the corresponding $F_{main}(x,y)$ and$F_{fine}(x,y)$. To finely segment blood vessels, $F_{main}(x,y)$ and $F_{fine}(x,y)$ are passed through a 1×1 convolution with a step size of 1 to fuse features and then activated by ReLu. Finally, according to Eq. (7), the obtained dual-channel prediction results are fused to realize the information complementation of thick and thin vessels. The final blood vessel segmentation map is obtained.

$$F_{fuse}(x,y) = \sum_{x=1}^{H}\sum_{y=1}^{W} F^1_{main}(x,y) \oplus F^1_{fine}(x,y) \tag{7}$$

where $\oplus$ represents the logical OR operation; $F_{fuse}(x,y)$ represents the blood vessel segmentation map after dual-channel fusion; $F^1_{mian}(x,y)$ and $F^1_{fine}(x,y)$ represents the blood vessel prediction images output by MainSegment-Net and FineSegment-Net, respectively.

Fig. 6 shows the blood vessel segmentation effect map of the dual-channel asymmetric CNN. Wherein, Fig. 6(a) and (b) represent the output segmentation map of MainSegment-Net and FineSegment-Net, respectively. Fig. 6 (c) represents the segmentation map of the dual-channel fusion. Fig. 6(d) shows a detailed view of the rectangle in Fig. 6(a-c). As shown in Fig. 6(a), areas 1 and 4 are missing a large number of thin vessels, but thick vessels are clearly defined. From Fig. 6(b), areas 2 and 5 are rich in detail, but thick vessels are relatively blurred. Fig. 6(a) and (b) are used for information fusion. The fine segmentation map is used to supplement the lack of details in the main segmentation map to obtain a complete and clear retinal vessel segmentation map (Fig. 6(c)).

3.5. *Network training*

The MainSegment-Net and FineSegment-Net models were developed and designed based on the PyTorch framework under the Ubuntu16.0 system. A 1080Ti graphics card was used to train and test the asymmetric CNN. Adam algorithm was adopted to optimize the parameters in the dual-channel network during training, and cross-entropy was selected as the loss function, as shown in Eq. (8) [28].

$$Loss = -\frac{1}{N}\sum_{i}^{N}\left[x_i \log p_i + (1-x_i)\log(1-p_i)\right] \tag{8}$$

where N represents the total number of pixels in the image, and i represents the number of classifications. The retinal blood vessel segmentation belongs to the binary classification problem of per-pixel recognition. x_i represents the probability value of the background pixel under the gold label, 1- x_i represents the probability value of the blood vessel pixel under the gold label, and p_i represents the probability value obtained from the Sigmoid function mapping of the prediction map.

Considering the small sample size of the selected databases, our experiment improved the dual-channel network performance by increasing the number of the training. During the training of the network, all input images and labels are randomly deducted from the patch with blood vessels and

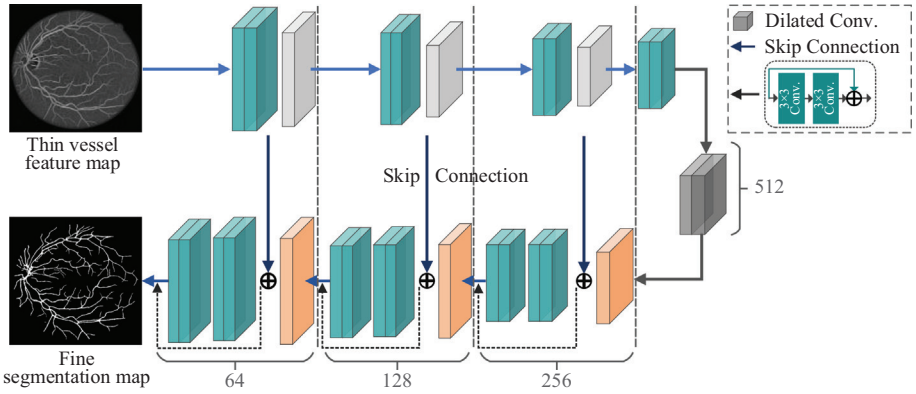

Fig. 5 – Structure diagram of FineSegment-Net.

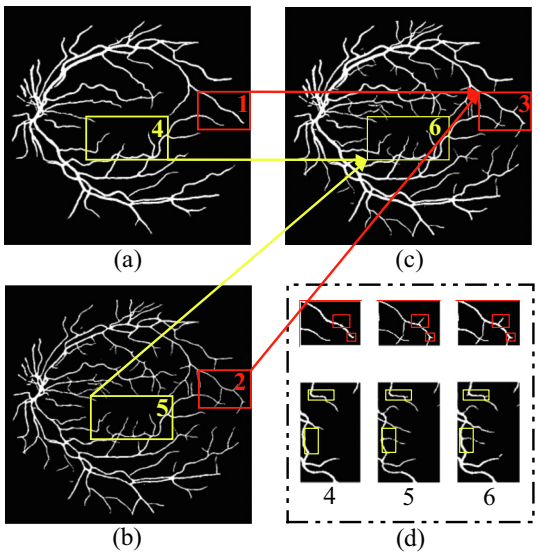

Fig. 6 – The blood vessel segmentation effect map of the dual-channel asymmetric CNN: (a) Segmentation map output by MainSegment-Net; (b) segmentation map output by FineSegment-Net; (c) segmentation map after information fusion; (d) detail view of the rectangles in (a)-(c).

then scaled to 512 × 512. Set the initial learning rate to 0.01 and decay exponentially, the batch size to 4, and a total of 200 training iterations.

4. Experimental results

4.1. *Database*

Digital fundus camera images from two common databases, DRIVE [29] and CHASE_DB1 [30], are selected as experimental subjects. The DRIVE database composed by Nieneijer in 2004 consists of 40 color fundus images (565 × 584 pixels), divided into the training and test sets with 20 images each. The CHASE_DB1 database extracted from the Children's Heart and Health Research Center consists of 28 color fundus images (999 × 960 pixels), collected from the left and right eyes of 14 children, of which 20 images are used for training, and eight images are used for testing. Compared with the DIVE database, the CHASE_DB1 original images are characterized by low illumination and contrast. Each image in the two databases corresponds to the manual segmentation maps of two experts, this paper chooses the first expert manual annotation as the segmentation standard.

4.1.1. *DRIVE database*

Five fundus images with different characteristics are selected for comparative analysis from 20 images in the test set of the DRIVE database. The first image has a moderate contrast and clear vessels; the second has high contrast and heterogeneous capillary branches; the third has low contrast and many capillaries; the fourth shows more branched and heterogeneous vessels; the fifth contains diseased blood vessels and severe impurity interference. To facilitate horizontal comparison of the methods, the experimental results of the retinal vessel segmentation method proposed in paper [31] are presented. As shown in Fig. 7, the first row contains the original images in the DRIVE database; the second row contains the standard maps of blood vessels manually segmented by the first expert; the third row contains the segmentation maps obtained by the method of paper [31], and the fourth row contains the segmentation maps obtained by the proposed method in this paper.

The method proposed in paper [31] used a directional triple-stick filtering and a Block Matching 3D (BM3D) filter to boost the detection of tiny and large vessels, respectively, which can boost the accuracy of large vessels detection and ensure effective perception of tiny vessels. However, the directional triple-stick filtering easily filters out some tiny vessels, and the segmentation of large vessels is still not accurate enough. We use the bilateral asymmetric convolutional neural network to segment blood vessel features, which can detect thick and thin vessels more accurately and completely.

4.1.2. *CHASE_DB1 database*

Four fundus images are randomly selected from 8 images in the test set of the CHASE_DB1 database, as shown in Fig. 8. Here, the first row contains the original images, and the second row contains the standard maps of blood vessel manually segmented by the first expert. The third and fourth rows contain the segmentation maps of the method proposed in paper [3] and our method, respectively.

The method proposed in paper [3] performed frequency division processing on fundus images through Gaussian filter, and inputted high and low frequency information into the multi-path convolutional neural network for feature extraction, which can achieve fast segmentation of low-dimensional features and ensure effective perception of high-dimensional features. However, the multi-path network does not fully consider the correlation between convolutional levels during the training process, and is not sufficiently targeted for high and low frequency information. It only uses channel number combination to achieve feature fusion, which leads to serious missed detection of thin vessels. We construct MainSegment-Net and FineSegment-Net based on the unique characteristics of thick and thin vessels, and adopts the step-by-step connection mode and the skip connection mode to connect the encoder and decoder respectively, which can effectively reduce the loss of thin vessels.

From the results of Figs. 7 and 8, it can be concluded that the method proposed in paper [31] cannot guarantee the integrity and connectivity of the blood vessel main part, and a large number of thin vessels are seriously lost, which leads to poor segmentation. The method proposed in paper [3] extracts high and low frequency information through a multi-path CNN, and the detection effect is improved, but it is still unable to accurately segment thin vessels. Our method adaptively extracts blood vessels through a 2D Gabor filter, and the processing methods of thick and thin vessels are greatly different, which not only ensure the integrity and connectivity of thick vessel, but also retain a large number of branches of thin vessels. Therefore, our method has better segmentation effect compared with other compared methods.

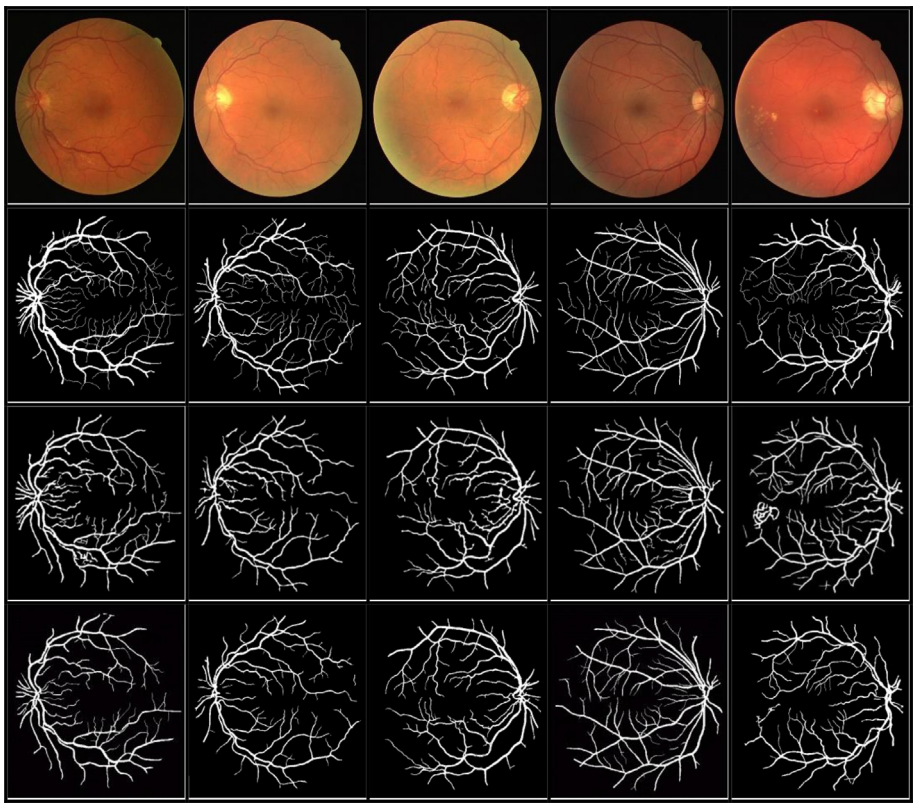

Fig. 7 – DRIVE database segmentation results. 1st row: original images; 2nd row: manual segmentation maps; 3rd row: segmentation maps of the method proposed in paper [31]; 4th row: segmentation maps of the method proposed in this paper.

4.2. *Quantitative analysis*

To further quantify the performance of our method, the following three indexes are used to evaluate the test sets in DRIVE and CHASE_DB1 databases. Here, *SE* represents sensitivity, *SP* represents specificity, and *Acc* represents accuracy, as shown in Eqs. (9)–(11).

$$SE = \frac{T_P}{T_P + F_N} \tag{9}$$

$$SP = \frac{T_N}{T_N + F_P} \tag{10}$$

$$Acc = \frac{T_N + T_P}{T_N + T_P + F_N + F_P} \tag{11}$$

where T_P represents true positive, referring to the number of blood vessel pixels correctly segmented; T_N represents true negative, referring to the number of background pixels correctly segmented; F_P represents false positive, referring to the number of blood vessel pixels wrongly segmented. F_N represents false negative, referring to the number of background pixels wrongly segmented. Additionally, ROC curve uses the false positive rate and true positive rate as the abscissa and ordinate, reflecting the changes of the two under different thresholds. Therefore, ROC curve is also used as an important index for measuring segmentation performance. The closer the area value under ROC curve (Auc) is to 1, the better the segmentation performance of the method. The objective comparison results produced by different methods are shown in Tables 1 and 2.

As can be seen from Table 1, the evaluation indexes Acc, SE, SP, and Auc of our method on the DRIVE database are 0.9630, 0.8745, 0.9823, and 0.9670, respectively. Our method has achieved a balance between sensitivity and specificity, while obtaining the second best overall accuracy. Compared with unsupervised methods, all evaluation indexes of our method are both in the lead. Compared with supervised methods, although the Acc of our method is not as good as the method in the literature [8], the SE and SP of our method are better. From all supervised methods in Table 1, they usually sacrifice sensitivity for higher specificity and accuracy.

Similarly, it can be seen from Table 2 that the evaluation indexes Acc, SE, SP, and Auc of our method on the CHASE_DB1 database are 0.9694, 0.8916, 0.9794, and 0.9677, respectively. Compared with other methods, our method has the highest accuracy. The method of Li et al. [35] obtained the highest Auc and specificity, but its sensitivity was much lower than other methods. In addition, the methods of Khan [31] and Yan [34] obtained high accuracy at the cost of low specificity.

5. Discussion

Fig. 9 shows the Box-and-Whisker statistical results of Acc, SE, SP, and Auc of different methods in the retinal vessel segmentation of images on the DRIVE database. It can be

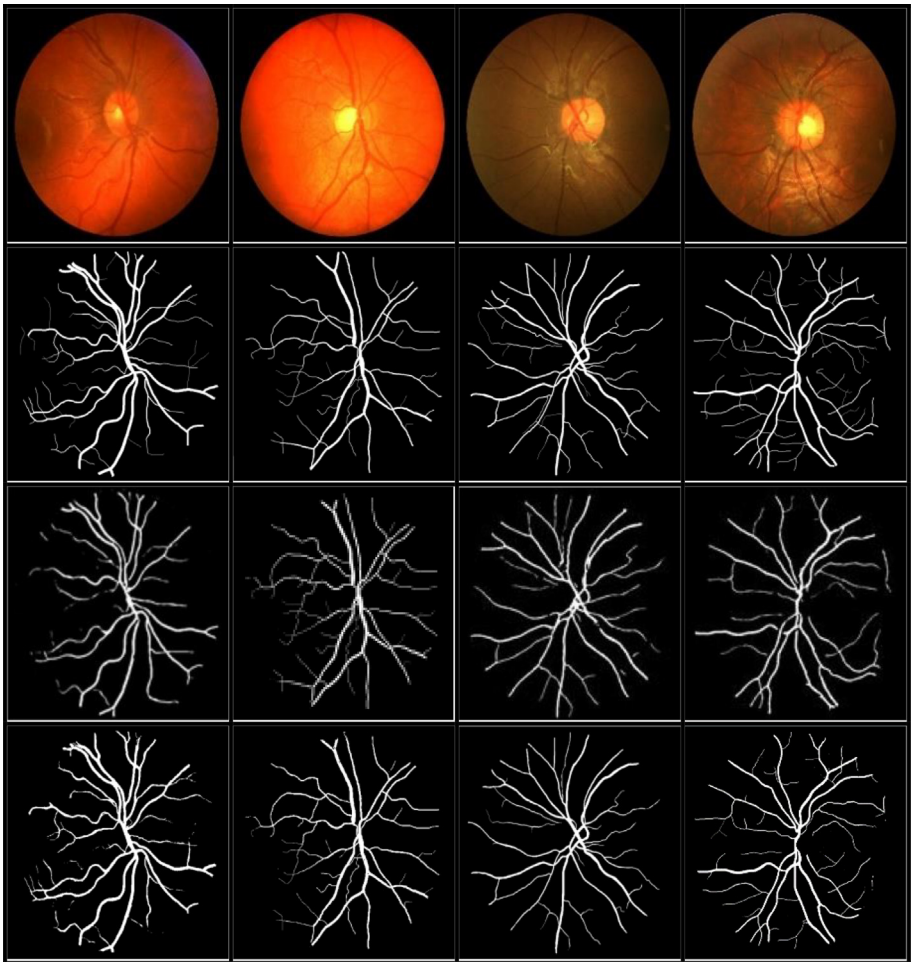

Fig. 8 – CHASE_DB1 database segmentation results. 1st row: original images; 2nd row: manual segmentation maps; 3rd row: segmentation maps of the method proposed in [3]; 4th row: segmentation maps of the method proposed in this paper.

Table 1 – Comparison made with other methods on the basis of DRIVE database in terms of SE, SP, Acc, and Auc.

Type	Methods	Year	Acc	SE	SP	Auc
Unsupervised	Geetharamani et al. [16]	2016	0.9536	0.7079	0.9778	0.8528
	Farokhian et al. [4]	2017	0.9392	0.6933	0.9777	0.9530
	Hugo et al. [11]	2018	0.8758	0.7854	0.9662	0.9503
	Khawaja et al [32]	2019	0.9553	0.8043	0.9730	0.9621
	Tian et al. [15]	2021	0.9554	0.6942	0.9802	0.9714
	Khan et al. [31]	2021	0.9610	0.8125	0.9763	0.9730
Supervised	Peng et al. [33]	2018	0.9629	0.8112	0.9843	0.9841
	Yan et al. [34]	2018	0.9542	0.7653	0.9818	0.9752
	Tian et al. [3]	2020	0.9580	0.8639	0.9690	0.9560
	Samuel et al. [6]	2021	0.9627	0.7827	0.96821	0.9789
	Tchinda et al. [5]	2021	0.9480	0.7352	0.9775	0.9678
	Li et al. [8]	2021	0.9698	0.7931	0.9896	0.9738
	Proposed		0.9630	0.8745	0.9823	0.9670

observed that Reference [33] proposed a CDNet model based on U-Net and deconvolution, but only verified the performance of the network on the DRIVE database, which could not objectively reflect the generalization ability of the algorithm; the evaluation indexes Acc, SE, and SP of this method on the DRIVE database are 0.9629, 0.8112, and 0.9843, respectively, which are all lower than the evaluation indexes of our method. Reference [34] considered the unbalanced pixel ratio of thick and thin blood vessels, and uses segment-level and the pixel-wise losses to reduce losses during training; but the Acc and SE of this method on the DRVIE database are inferior, which are 0.9542 and 0.7653 respectively. Reference [3]

Table 2 – Comparison made with other methods on the basis of CHASE_DB1 database in terms of SE, SP, Acc, and Auc.

Type	Methods	Year	Acc	SE	SP	Auc
Unsupervised	Li et al. [35]	2016	0.9581	0.7507	0.9793	0.9716
	Khawaja et al. [32]	2019	0.9528	0.7974	0.9697	0.9687
	Khan et al. [31]	2021	0.9578	0.8012	0.9730	0.9708
Supervised	Yan et al. [34]	2018	0.9610	0.7633	0.9809	0.9718
	Tian et al. [3]	2020	0.9601	0.8778	0.9680	0.9577
	Tchinda et al. [5]	2021	0.9452	0.7279	0.9658	0.9681
	Proposed		0.9694	0.8916	0.9794	0.9677

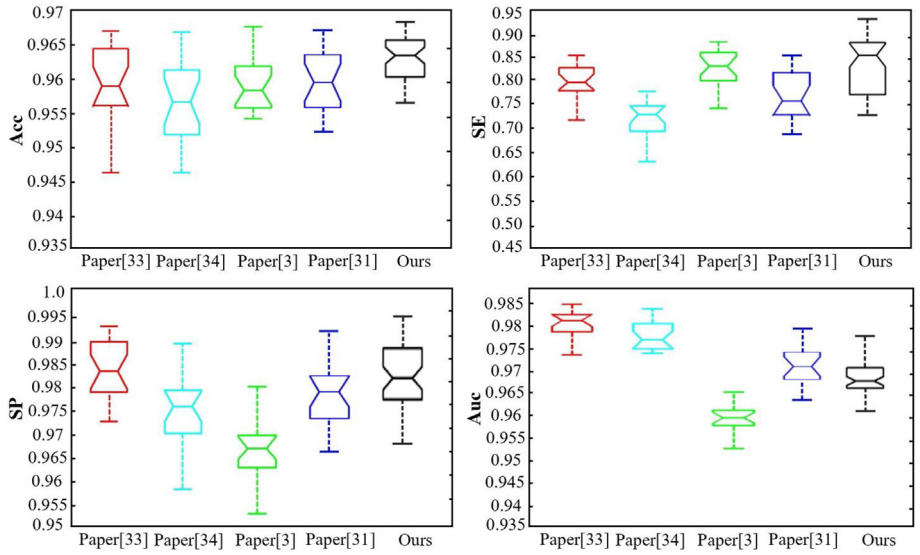

Fig. 9 – Box plot statistics for different evaluation results of the evaluation indicators for the DRIVE dataset.

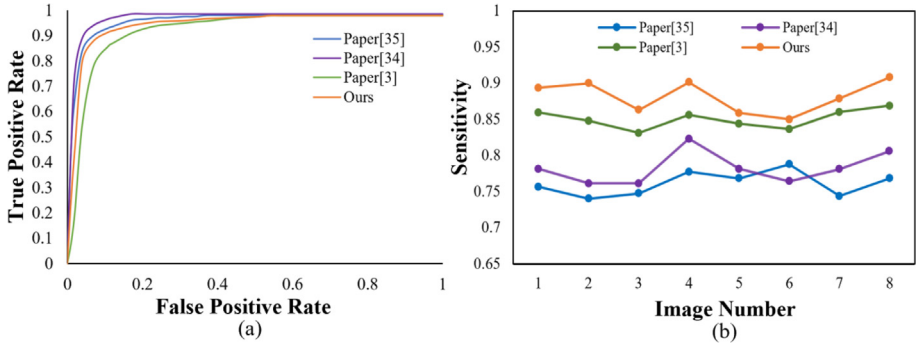

Fig. 10 – Comparison of the performance of different retinal blood vessel segmentation algorithms: (a) ROC curves; (b) SE for the test set of the CHASE_DB1 database.

constructed low-frequency feature extraction path and high-frequency feature extraction path for High and Low frequency information of blood vessels, and obtained fine blood vessels through multi-path fusion; but high-frequency information extraction is not sufficient due to the small difference between multiple paths. The evaluation indexes Acc, SE, SP, and Auc of this method on the DRIVE database are 0.9580, 0.8639, 0.9690, and 0.9560, respectively, which are 0.005, 0.0106, 0.0133, and 0.011 lower than the evaluation indicators of our method.

Reference [31] used a directional triple-stick filtering and a Block Matching 3D (BM3D) filter to boost the detection of tiny

and large vessels, respectively; but the directional triple-stick filtering easily filters out some tiny vessels, which makes the evaluation indexes Acc, SE, and SP of this method are all lower than those of our method. In contrast, our method can ensure the box is at a reasonable length while obtaining the best Acc and has better stability and segmentation effect.

In addition, it can be seen from the ROC curve of Fig. 10(a) that the ROC curve of our method is biased towards the upper left area of the coordinate system, and our method is better than the method of the literature [3]. As it can be seen from Table 2, the Auc value of the algorithm in this paper is 0.9677, which is slightly higher than 0.9577 in the literature [3]. Although the ROC curve of our method is slightly lower than that in the literatures [34] and [35], it can be seen from Fig. 10(b) that the sensitivity of our method is better than other methods. From Table 2, the sensitivity of the literature [34] and [35] are 0.7633 and 0.7507, respectively. The sensitivity of this paper is 0.8916, which is significantly higher than several other comparison methods. In contrast, the sensitivity of the proposed method is better, which further proves that the segmentation results of our method have obvious advantages, and the overall segmentation effect is better.

6. Conclusion

Considering the wide scale range of blood vessels in fundus images, it is not easy to integrate different blood vessel information into the unified image representation and pixel classification system. Therefore, we propose a retinal blood vessel segmentation method based on the dual-channel asymmetric CNN. First, after performing vascular enhancement on retinal images, a multi-directional and multi-scale 2D Gabor filter is used to adaptively extract the thick and thin vessel feature maps. Then, the asymmetric CNN, MainSegment-Net and FineSegment-Net, is constructed. MainSegment-Net introduces the step-by-step connection mode to simplify the convolutional layer to achieve rapid positioning and segmentation of thick vessels. However, FineSegment-Net adopts the skip connection mode to combine the low-level feature map of the encoder with the high-level feature map of the decoder step-by-step to improve the accuracy of thin vessel segmentation. Finally, the information of the dual-channel network is fused to obtain the final vascular segmentation map. The feasibility of the proposed network model is verified on DRIVE and CHASE_DB1 databases. The experimental results demonstrate that the proposed method has the advantage of accurate segmentation, and the blood vessels are relatively complete and continuous, which is significantly better than other comparison methods. Therefore, the proposed method has a good application prospect in medical image processing and provides a new idea for subsequent fundus image processing and analysis.

Conflict of interest statement

We declare that there is no conflict of interests regarding the publication of this article

REFERENCES

[1] Prasad Reddy PVGD. Blood vessel extraction in fundus images using hessian eigenvalues and adaptive thresholding. Evol Intel 2021;14(2):577–82.

[2] Ramos-Soto O, Rodríguez-Esparza E, Balderas-Mata SE, Oliva D, Hassanien AE, Meleppat RK, et al. An efficient retinal blood vessel segmentation in eye fundus images by using optimized top-hat and homomorphic filtering. Comput Methods Prog Biomed 2021;201. 105949.

[3] Tian C, Fang T, Fan Y, Wu W. Multi-path convolutional neural network in fundus segmentation of blood vessels. Biocybern Biomed Eng 2020;40(2):583–95.

[4] Farokhian F, Yang C, Demirel H, Wu S, Beheshti I. Automatic parameters selection of Gabor filters with the imperialism competitive algorithm with application to retinal vessel segmentation. Biocybern Biomed Eng 2017;37(1):246–54.

[5] Tchinda BS, Tchiotsop D, Noubom M, Louis-Dorr V, Wolf D. Retinal blood vessels segmentation using classical edge detection filters and the neural network. Inform Med Unlock 2021;23(3). 100521.

[6] Samuel PM, Veeramalai T. VSSC Net: Vessel Specific Skip chain Convolutional Network for blood vessel segmentation. Comput Methods Prog Biomed 2021;198. 105769.

[7] Oliveira A, Pereira S, Silva CA. Retinal vessel segmentation based on Fully Convolutional Neural Networks. Expert Syst Appl 2018;112:229–42.

[8] Li Z, Jia M, Yang X, Xu M. Blood vessel segmentation of retinal image based on Dense-U-Net Network. Micromachines 2021;12(12):1478.

[9] Liu C, Gu P, Xiao Z, Tang J. Multiscale U-Net with spatial positional attention for retinal vessel segmentation. J Healthc Eng 2022;2022:1–10.

[10] Chaudhuri S, Chatterjee S, Katz N, Nelson M, Goldbaum M. Detection of blood vessels in retinal images using two-dimensional matched filters. IEEE Trans Med Imaging 1989;8 (3):263–9.

[11] Hugo AR, Gabriel ACJ, Ivan CA, José RP, Sergio L. Blood vessel segmentation in retinal fundus images using Gabor filters, fractional derivatives, and Expectation Maximization. Appl Math Comput 2018;339:568–87.

[12] Luo ZL, Jia Y. The comparison of retinal vessel segmentation methods in fundus images. J Phys Conf Ser 2020;1574. 012160.

[13] Delibasis KK, Kechriniotis AI, Tsonos C, Assimakis N. Automatic model-based tracing algorithm for vessel segmentation and diameter estimation. Comput Methods Prog Biomed 2010;99(2):108–22.

[14] Zhao J, Yang J, Ai D, Song H, Jiang Y, Huang Y, et al. Automatic retinal vessel segmentation using multi-scale superpixel chain tracking. Digit Signal Process 2018;81:26–42.

[15] Tian F, Li Y, Wang J, Chen W, Hemanth J. Blood vessel segmentation of fundus retinal images based on improved frangi and mathematical morphology. Comput Math Methods Med 2021;2021:1–11.

[16] Geetharamani R, Balasubramanian L. Retinal blood vessel segmentation employing image processing and data mining techniques for computerized retinal image analysis. Biocybern Biomed Eng 2016;36(1):102–18.

[17] Ding JQ, Zhang ZH, Tang JJ, Guo F. A multichannel deep neural network for retina vessel segmentation via a fusion mechanism. Front Bioeng Biotech 2021;9. 697915.

[18] Orlando JI, Prokofyeva E, Blaschko MB. A discriminatively trained fully connected conditional random field model for blood vessel segmentation in fundus images. IEEE Trans Biomed Eng 2017;64(1):16–27.

[19] Fu H, Xu Y, Wong DWK, Liu J. Retinal vessel segmentation via deep learning network and fully-connected conditional

random fields. In: IEEE 13th International Symposium on Biomedical Imaging (ISBI). p. 698–701.
[20] Long J, Shelhamer E, Darrell T. Fully convolutional networks for semantic segmentation. IEEE Trans Pattern Anal Mach Intell 2017;39(4):640–51.
[21] Ronneberger O, Fischer P, Brox T. U-net: Convolutional networks for biomedical image segmentation. Medical Image Comput Comput-Assisted Intervention 2015;9351:234–41.
[22] Gu Z, Cheng J, Fu H, Zhou K, Hao H, Zhao Y, et al. CE-Net: Context encoder network for 2D medical image segmentation. IEEE Trans Med Imaging 2019;38(10):2281–92.
[23] Pan X, Zhang Q, Zhang H, Li S. A fundus retinal vessels segmentation scheme based on the improved deep learning U-Net model. IEEE Access 2019;7:122634–43.
[24] Cloutman LL. Interaction between dorsal and ventral processing streams: Where, when and how? Brain Lang 2013;127(2):251–63.
[25] Pathan S, Kumar P, Pai R, Bhandary SV. Automated detection of optic disc contours in fundus images using decision tree classifier. Biocybern Biomed Eng 2019;40(1):52–64.
[26] Spratling MW. Image segmentation using a sparse coding model of cortical area V1. IEEE Trans Image Process 2013;22 (4):1631–43.
[27] Fang A, Zhao X, Zhang Y. Cross-modal image fusion guided by subjective visual attention. Neurocomputing 2020;414:333–45.
[28] David SA, Mahesh C, Kumar VD, Polat K, Alhudhaif A, Nour M, et al. Retinal blood vessels and optic disc segmentation using U-Net. Math Probl Eng 2022;2022:1–11.
[29] Staal J, Abràmoff MD, Niemeijer M, Viergever MA, Ginneken BV. Ridge-based vessel segmentation in color images of the retina. IEEE Trans Med Imaging 2004;23(4):501–9.
[30] Fraz MM, Remagnino P, Hoppe A, Uyyanonvara B, Rudnicka AR, Owen CG, et al. An ensemble classification-based approach applied to retinal blood vessel segmentation. IEEE Trans Biomed Eng 2012;59(9):2538–48.
[31] Khan TM, Khan MAU, Rehman NU, Naveed K, Afridi IU, Naqvi SS, et al. Width-wise vessel bifurcation for improved retinal vessel segmentation. Biomed Signal Process Control 2022;71.
[32] Khawaja A, Khan TM, Khan MAU, Nawaz SJ. A multi-scale directional line detector for retinal vessel segmentation. Sensors 2019;19(22):4949.
[33] Peng S, Zheng C, Xu F, Xiao H, Nam HD, Wu Y. Blood vessels segmentation by using CDNet. In: IEEE 3rd International Conference on Image, Vision and Computing (ICIVC). p. 305–15.
[34] Yan Z, Yang X, Cheng KTT. Joint segment-level and pixel-wise losses for deep learning based retinal vessel segmentation. IEEE Trans Biomed Eng 2018;65(9):1912–23.
[35] Li Q, Feng B, Xie LP, Liang P, Zhang H, Wang T. A Cross-modality Learning Approach for Vessel Segmentation in Retinal Images. IEEE Trans Med Imaging 2016;35(1):109–18.